

Tunable surface electron gas and effect of phonons in Sr_2CuO_3 : A first-principles study

Xin Du^{1,2}, Hui-Hui He^{1,2}, Xiao-Xiao Man^{1,2}, Zhong-Yi Lu^{1,2,*} and Kai Liu^{1,2†}

¹*School of Physics and Beijing Key Laboratory of Opto-electronic Functional Materials & Micro-nano Devices, Renmin University of China, Beijing 100872, China*

²*Key Laboratory of Quantum State Construction and Manipulation (Ministry of Education), Renmin University of China, Beijing 100872, China*

(Dated: November 21, 2024)

While the conducting CuO_2 planes in cuprate superconductors have been widely recognized as a crucial component in producing high superconducting T_c , recent experimental and theoretical studies on $\text{Ba}_{2-x}\text{Sr}_x\text{CuO}_{3+\delta}$ have also drawn much attention to the importance of Cu-O chains in one-dimensional (1D) cuprates. To better understand the cuprates containing Cu-O chains, here we have studied the electronic, magnetic, and phonon properties of Sr_2CuO_3 bulk and films based on the spin-polarized density functional theory calculations. We first reproduced the typical Mott insulator feature of the cuprate parent compound for bulk Sr_2CuO_3 , and then built a Sr_2CuO_3 thin film with Cu-O chains exposed on the surface to directly investigate their characteristics. Different from the insulating bulk phase, the Sr_2CuO_3 surface shows interesting metallic properties. Further electronic structure calculations reveal the existence of spin-polarized electron gas between surface Sr atoms that strongly depends on the interchain coupling of Cu spins. Moreover, the phonon modes that involve the vibrations of in-chain and out-of-chain O atoms can induce strong charge and spin fluctuations in the surface layer of Sr_2CuO_3 film, which suggests significant multiple degree-of-freedom couplings that may be important for the superconductivity in 1D cuprates. Our work provides a comprehensive viewpoint of the properties of Cu-O chains in Sr_2CuO_3 , facilitating a complete understanding of 1D cuprate superconductors.

I. INTRODUCTION

Cuprates, serving as the superconducting family with the highest superconducting transition temperature (T_c) at ambient pressure [1–3], have been one of the most important topics in condensed matter physics over the past decades [4–9]. Despite extensive studies conducted to explore the conducting two-dimensional (2D) CuO_2 planes, which are generally accepted to play an active role in high T_c [10, 11], the origin of high-temperature superconductivity still remains a puzzle. On the other hand, in the history of superconductors, plenty of quasi-one-dimensional (1D) superconductors have also been reported [12–17]. Therefore, in addition to the cuprates with 2D CuO_2 planes, the cuprates with the simple basic unit of 1D Cu-O chains may provide another opportunity to explore the microscopic mechanism of unconventional superconductivity.

Several alkaline-earth cuprates without intact 2D CuO_2 planes have manifested superconductivity [17–19]. Early high-pressure experiments reported the synthesis of $\text{Sr}_{n+1}\text{Cu}_n\text{O}_{2n+1+\delta}$ compounds and refined $\text{Sr}_2\text{CuO}_{3.1}$ ($n = 1$, $T_c \sim 70$ K) with a K_2NiF_4 type structure [17]. Subsequent neutron powder diffraction and electron diffraction measurements suggested that oxygen vacancies reside mainly on the CuO_2 planes [20, 21]. Later on, the Cu K-edge x-ray absorption fine structure (XAFS) studies revealed that the structure of highly overdoped superconductor $\text{Sr}_2\text{CuO}_{3.3}$ ($T_c \sim 95$ K) does not contain

complete CuO_2 planes [18, 22]. Similarly, our computational study [23] on a newly synthesized cuprate superconductor $\text{Ba}_2\text{CuO}_{3+\delta}$ [19] also suggested that oxygen vacancies prefer to reside in the planar sites rather than the apical sites, emphasizing the Cu-O chain structure in $\text{Ba}_2\text{CuO}_{3+\delta}$. Moreover, recent angle-resolved photoemission spectroscopy (ARPES) experiments on $\text{Ba}_{2-x}\text{Sr}_x\text{CuO}_{3+\delta}$ [24] found an additional strong near-neighbor attraction, which may be attributed to the electron-phonon (*el-ph*) interaction, and the subsequent theoretical modeling work highlighted the effect of the O phonon modes in the Cu-O chains [25]. The above studies imply that the 1D Cu-O chains, beyond the well-known 2D CuO_2 planes, may play an unexpected role in some alkaline-earth cuprates with high superconducting T_c . Among the alkaline-earth cuprates with perfect 1D Cu-O chains, Sr_2CuO_3 has been intensively investigated as an ideal 1D Heisenberg $S = 1/2$ antiferromagnetic (AFM) system [26–29]. Nevertheless, there is much less research on the couplings between multiple degrees of freedom in Sr_2CuO_3 , which may be indispensable for a complete understanding of the exotic physical properties of 1D cuprates.

In this work, we have performed first-principles calculations to explore the lattice dynamics, electronic structure, as well as magnetic and phonon properties of Sr_2CuO_3 bulk and films. After checking the Mott insulating behavior of bulk phase, we studied the electronic structure and magnetism of Sr_2CuO_3 film with Cu-O chains exposed on the surface. Notably, we find the spin-polarized electron gas between surface Sr atoms depending on the interchain coupling of Cu spins. Furthermore, we investigated the effects of phonon and surface modification on the electronic and magnetic properties of sur-

* zlu@ruc.edu.cn

† kliu@ruc.edu.cn

face Cu-O chains. Our findings about the tunable spin-polarized electron gas on surface and multiple-degree-of-freedom couplings of Sr_2CuO_3 film call for future experimental examination.

II. COMPUTATIONAL DETAILS

The structural, electronic, and magnetic properties of Sr_2CuO_3 bulk and films were studied by using the spin-polarized density functional theory (DFT) calculations [30, 31] with the generalized gradient approximation (GGA) of the Perdew-Burke-Ernzerhof (PBE) functional [32], as implemented in the Vienna *ab initio* simulation package (VASP) [33]. The projector augmented wave (PAW) [34] potentials with valence electron configurations of $4s^2 4p^6 5s^2$, $3d^{10} 4s^1$, and $2s^2 2p^4$ were adopted for Sr, Cu, and O atoms, respectively. The kinetic energy cutoff of the plane wave basis was set to 520 eV. Monkhorst-Pack \mathbf{k} -meshes [35] of $8 \times 8 \times 4$ and $4 \times 6 \times 1$ were used for the $\sqrt{2} \times \sqrt{2} \times 1$ bulk supercell and the thin films, respectively. All atomic positions were fully relaxed until the forces on atoms were smaller than 0.01 eV/Å and the energy convergence criterion was set to 10^{-6} eV. For the 7-layer Sr_2CuO_3 slab, the vacuum layer was set to 15 Å in order to eliminate the artificial interactions among the image slabs along the (001) direction. Actually, we tested 20-Å and 25-Å vacuum layers to ensure that the vacuum layer of 15 Å is thick enough to achieve good convergence. The effective Hubbard U of 6.5 eV, which has been applied to the isostructural compound Ba_2CuO_3 [23], was utilized to describe the strong correlation effect among Cu $3d$ electrons throughout all calculations. With $U_{\text{eff}} = 6.5$ eV, the lattice constants and band gap of the AFM ground state as well as the magnetic exchange strength (Tables S1, S2, and S3 in the Supporting Information (SI) [36]) are in good accordance with the experimental values [26, 37–39]. The influence of the van der Waals interaction in the bare and I-absorbed Sr_2CuO_3 surfaces (films) was examined with the DFT-D2 method [40, 41]. Here, the spin-exchange interaction was determined based on an effective Heisenberg model [42–44]: $H = J_{\perp} \sum_{\langle ij \rangle} \vec{S}_i \cdot \vec{S}_j + J_{\parallel} \sum_{\langle\langle ij \rangle\rangle} \vec{S}_i \cdot \vec{S}_j$, where J_{\perp} and J_{\parallel} denote the respective couplings between the interchain and in-chain Cu spins, and S is the local magnetic moment on Cu. The phonon properties were investigated via the frozen phonon approach [45]. The polarization vector components $e_{\alpha i}^s$ (α : atomic label; $i = x, y, z$) of phonon modes s were calculated through diagonalizing the dynamical matrix [46]. As introduced in our previous work on SrCuO_2 [47], in a specific phonon mode s with frequency ω_s , the atoms could be displaced away from their equilibrium positions by $\pm \sqrt{2(n+1/2)\hbar/m_{\alpha} \omega_s} e_{\alpha i}^s$ ($n = 1$ corresponds to a potential energy of $3\hbar\omega_s/2$) along two opposite directions of the normal-mode coordinates. By this means, we could compare the physical properties of the structures with atomic displacements and those at equilibrium positions.

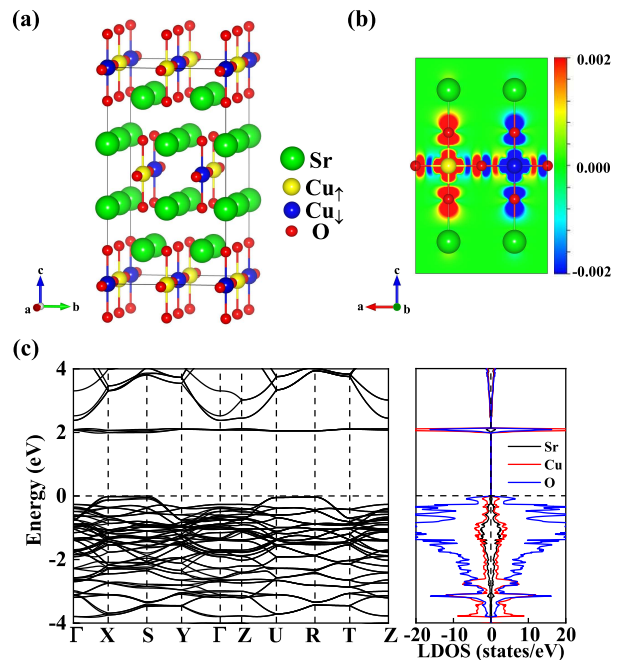


FIG. 1. (Color online) (a) Crystal structure, (b) spin density map, (c) electronic band structure and local density of states (LDOS) of bulk Sr_2CuO_3 in the AFM Néel state. The green and red balls represent Sr and O atoms, respectively. The yellow and blue balls denote the spin-up and spin-down Cu atoms, respectively. The two-dimensional (2D) spin density map is the (010) plane cut from the three-dimensional (3D) plot, and the color bar in (b) is in units of $e/\text{Å}^3$.

III. RESULTS AND DISCUSSION

A. Crystal structure, magnetic configuration, and electronic properties of bulk Sr_2CuO_3

Figures 1a and S1 of SI [36] show the crystal structure of Sr_2CuO_3 , where the Sr-O, Cu-O, and Sr-O layers form a sandwich structure along the c direction. Each Cu atom is coordinated with four O atoms, forming Cu-O chains along the a direction. Because of the partially occupied Cu $3d$ orbitals, the nonmagnetic (NM), ferromagnetic (FM), and three antiferromagnetic (AFM) states (Néel, AFM1, and stripe) were considered to study the magnetic configurations of Sr_2CuO_3 . In the AFM Néel, AFM1, and stripe AFM states, the intrachain (interchain) couplings between Cu spins are AFM (AFM), AFM (FM), and FM (AFM), respectively (Fig. S1 of SI [36]). The total energies (with respect to that of the AFM Néel state) and the local magnetic moments on Cu atoms (M_{Cu}) for these magnetic states are shown in Table S3 of SI [36]. The calculation results indicate that the AFM Néel state is the magnetic ground state, whose energy is 0.6, 137.7, 138.3, and 245.2 meV/Cu lower than those of the AFM1, stripe AFM, FM, and NM states, respectively. Due to the weak interchain magnetic coupling, the total energies and

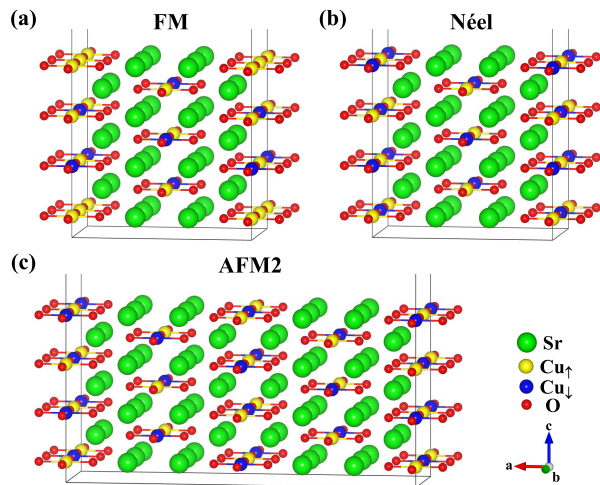


FIG. 2. (Color online) Crystal structure and typical magnetic configurations of the 7-layer Sr_2CuO_3 slab: (a) FM state, (b) AFM Néel state, and (c) AFM2 state. The green and red balls represent Sr and O atoms, respectively. The yellow and blue balls denote the spin-up and spin-down Cu atoms, respectively.

local moments M_{Cu} of the AFM Néel and AFM1 states, as well as those of the FM and stripe AFM states, are quite similar to each other.

We further explore the magnetic and electronic properties of Sr_2CuO_3 in the AFM Néel ground state (Fig. 1a). The spin density map plotted on the (010) plane clearly indicates that the Cu spins in each Cu-O chain are antiferromagnetically coupled along the a axis and the O atoms are also spin-polarized by the neighboring Cu atoms (Fig. 1b). The calculated band structure and local density of states (LDOS) well reproduce the Mott insulator feature with a band gap of 1.98 eV, while the conduction band minimum (CBM) and valence band maximum (VBM) are contributed by Cu and O orbitals, respectively (Fig. 1c) [39]. According to previous studies on cuprates [23, 48–50], various Hubbard U_{eff} values have been adopted to examine the above results of Sr_2CuO_3 . Our calculations suggest that the chosen U_{eff} values, either 5.0, 6.5, 7.0, or 8.0 eV, would not change the relative stability among the magnetic states (Table S3 in the SI [36]). Notably, the band gap ($E_g = 1.98$ eV) of the AFM Néel state and the exchange coupling strength ($J_1 = 275$ meV) calculated with $U_{\text{eff}} = 6.5$ eV (Tables S1 and S2 in the SI [36]) are in good agreement with the experimental values of 1.5 eV and 260 meV [37–39], respectively.

B. Structural, magnetic, electronic and phonon properties of Sr_2CuO_3 thin film

Our previous study on $\text{Ba}_2\text{CuO}_{3+\delta}$ has proposed that the Cu-O chains may play an important role in its superconducting pairing [23]. Recent experiments on the $\text{Ba}_{2-x}\text{Sr}_x\text{CuO}_{3+\delta}$ superconductor have suggested that an

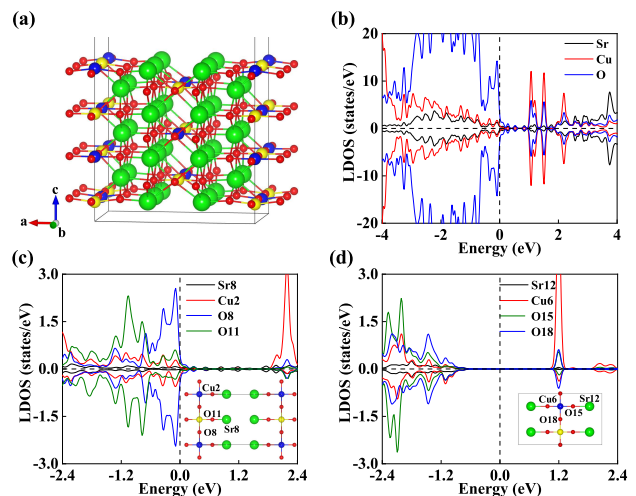


FIG. 3. (Color online) (a) Optimized crystal structure, (b) total, (c) surface-layer, and (d) inner-layer LDOS of Sr_2CuO_3 film in the AFM Néel ground state. The insets in (c) and (d) show the surface-layer and inner-layer structures, respectively.

additional strong interaction is attributed to the *el-ph* coupling in Cu-O chains [24, 25]. We noticed that pristine Sr_2CuO_3 film with Cu-O chains exposed on the surface could be grown by orientation-controlled epitaxy [51], and hence there is a chance to directly study the electronic, magnetic, and phonon properties of Cu-O chains on the surface of the Sr_2CuO_3 thin film.

1. Crystal structure and magnetic configurations of Sr_2CuO_3 thin film

We built a 7-layer Sr_2CuO_3 slab along the direction perpendicular to the Cu-O chains to simulate the Sr_2CuO_3 film (Fig. 2). Since the surface environment has changed in comparison with the bulk counterpart and may influence the magnetism of the top layer [52], we have checked the magnetic configurations for the surface layer of Sr_2CuO_3 film. To determine the magnetic ground state, the NM and FM states of surface atomic layers containing Cu-O chains are considered, while other inner layers maintain the AFM Néel state of bulk Sr_2CuO_3 (Fig. 2a). Two AFM states (AFM Néel and AFM2 states) are also considered, in which the intrachain nearest-neighbor couplings between Cu spins are both AFM, while the interchain couplings are FM (Fig. 2b) and AFM (Fig. 2c), respectively. The total energy calculations show that the NM state is unstable and the AFM Néel state cannot be distinguished from the AFM2 state due to the weak interchain coupling. The energy of the AFM Néel state is only 12 meV/Cu lower than that of the FM state (Table S4 of SI [36]). In comparison with the bulk value of 138 meV/Cu, this indicates that the magnetic competition (fluctuation) is much stronger on the surface.

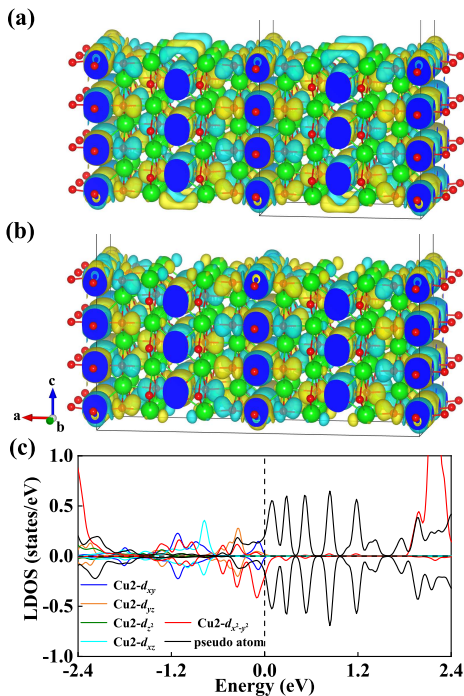


FIG. 4. (Color online) Spin density maps of Sr_2CuO_3 films in the (a) AFM Néel and (b) AFM2 states with the isosurface value of $0.0003 e/\text{\AA}^3$. (c) The LDOS of pseudo atom (locating between surface Sr atoms) and surface Cu2 atom [Fig. 3(c)] in the AFM Néel state.

2. Electronic and magnetic properties of Sr_2CuO_3 thin film

To explore the electronic properties of the Sr_2CuO_3 film in the AFM Néel ground state, the optimized crystal structure and LDOS are displayed in Figs. 3 and S2 of SI [36]. Unexpectedly, unlike the insulator feature of bulk phase (bandgap of 1.98 eV) as shown in Fig. 1c, the LDOS of Sr_2CuO_3 film in the AFM Néel ground state exhibits metallic properties (Fig. 3b). The layer-resolved DOS calculations show that only the surface layers are metallic and the states around the Fermi level are mainly contributed by O atoms (Fig. 3c), while the inner layers retain the Mott insulator behavior with a bandgap of ~ 1.62 eV (Fig. 3d). To better understand the origin of the metallicity, we analyzed the optimized crystal structure in detail (Fig. 3a). Although the chemical ratio of the surface layer is Sr:Cu:O = 2:1:3 as the bulk one, the lack of atoms on the vacuum side can cause the atomic distortion and the self-doping via the band bending of the surface layer, which lead to the metallic property. In addition, the results of the AFM2 state are quite similar to those of the AFM Néel state, and here we would not illustrate further (Fig. S2 of SI [36]).

Spin density maps of Sr_2CuO_3 film in the AFM Néel and AFM2 states are plotted in Figs. 4a, 4b, and S3 of SI [36]. Interestingly, in these two AFM states with similar total energy (Table S4 [36]) and electronic properties (Figs. 3 and S2 of SI [36]), the weak interchain

coupling of surface Cu spins has a large impact on the spin densities between surface Sr atoms. Specifically, for the AFM Néel state with FM interchain coupling, there are spin-polarized electron gases between two rows of surface Sr atoms, which show alternating spin-up and spin-down polarizations along the b axis (Figs. 4a, S3a, and S3c [36]). As for the AFM2 state, where the interchain coupling is AFM, there is no spin-polarized electron gas between two rows of surface Sr atoms (Figs. 4b, S3b, and S3d [36]). Compared with the bare spin density between Sr atoms in the bulk phase (Fig. 1b), these results indicate that the metallic surface of Sr_2CuO_3 film may have strong spin fluctuations due to the subtle interchain coupling. In addition, if a weak magnetic field is applied, the interchain interaction will favor the FM coupling instead of the AFM one, and would thus induce the appearance of spin-polarized electron gas between surface Sr atoms, i. e. the magnetic field can control the spin-polarized electron gas. We further added a pseudo atom to quantitatively describe the spin-polarized gas between two rows of surface Sr atoms in the AFM Néel state. The local magnetic moment of the pseudo atom is about $0.03 \mu_B$, which is an order of magnitude smaller than that of the Cu atom ($\sim 0.6 \mu_B$). The LDOS calculations suggest that the pseudoatom and the $3d$ orbitals of surface Cu2 atoms have comparable contributions around the Fermi level (Fig. 4c). Therefore, the intrinsic spin fluctuations and the controllable conductive spin-polarized electron gas make the surface of Sr_2CuO_3 (Fig. 2) an interesting platform for quantum state exploration.

3. Phonon effect on the electronic and magnetic properties of Sr_2CuO_3 thin film

Our recent study has revealed the notable role of O vibrations playing in the electronic and magnetic properties of the infinite-layer cuprate SrCuO_2 [47]; here we also focus on the phonon modes involving the surface O atoms in Sr_2CuO_3 film. For the 7-layer Sr_2CuO_3 slab, there are 84 atoms, corresponding to 252 phonon modes. The modes with considerable atomic displacements of surface O atoms are shown in Fig. 5, in which there are 4 and 8 phonon modes involving the vibrations of in-chain and out-of-chain O atoms, respectively. The in-chain O atoms have two vibration directions: along (Figs. 5d and 5i) and vertical to (Figs. 5c and 5k) the Cu-O chain (corresponding to the b and a axes, respectively). As for the out-of-chain (apical) O atoms, there are three vibration directions: along the b (Figs. 5f, 5g, 5h, and 5j), a (Figs. 5a, 5b, and 5e), and c (Fig. 5l) axes. In addition, the vibrations of the O atoms in the same or opposite directions can further lead to different vibrational patterns. Specifically, the bond-stretching (Fig. 5i) and apical O (Fig. 5e) phonon modes have been investigated in previous theoretical studies, which were proposed to be associated with the *el-ph* coupling in 1D cuprates [25, 53]. There are several phonon modes similar to the two above

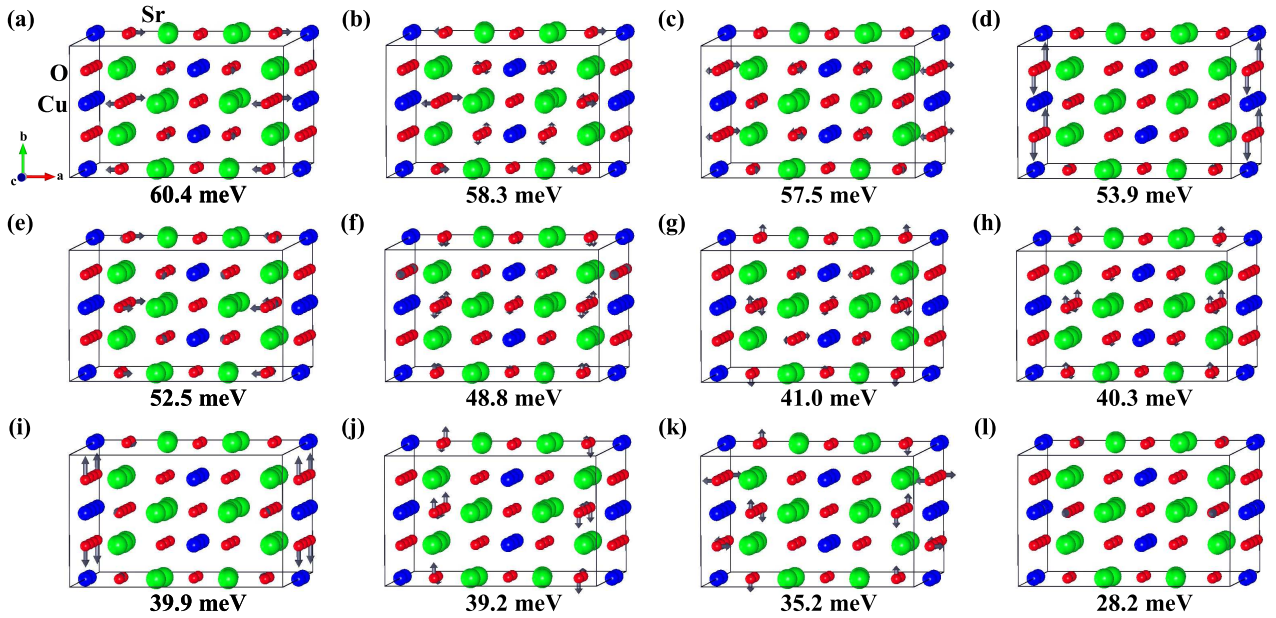


FIG. 5. (Color online) Top views of atomic displacement patterns for twelve optical phonon modes involving surface O atoms of Sr_2CuO_3 in the AFM Néel state. The gray arrows denote the directions and amplitudes of the atomic vibrations. The corresponding frequencies of the phonon modes are labeled in each panel.

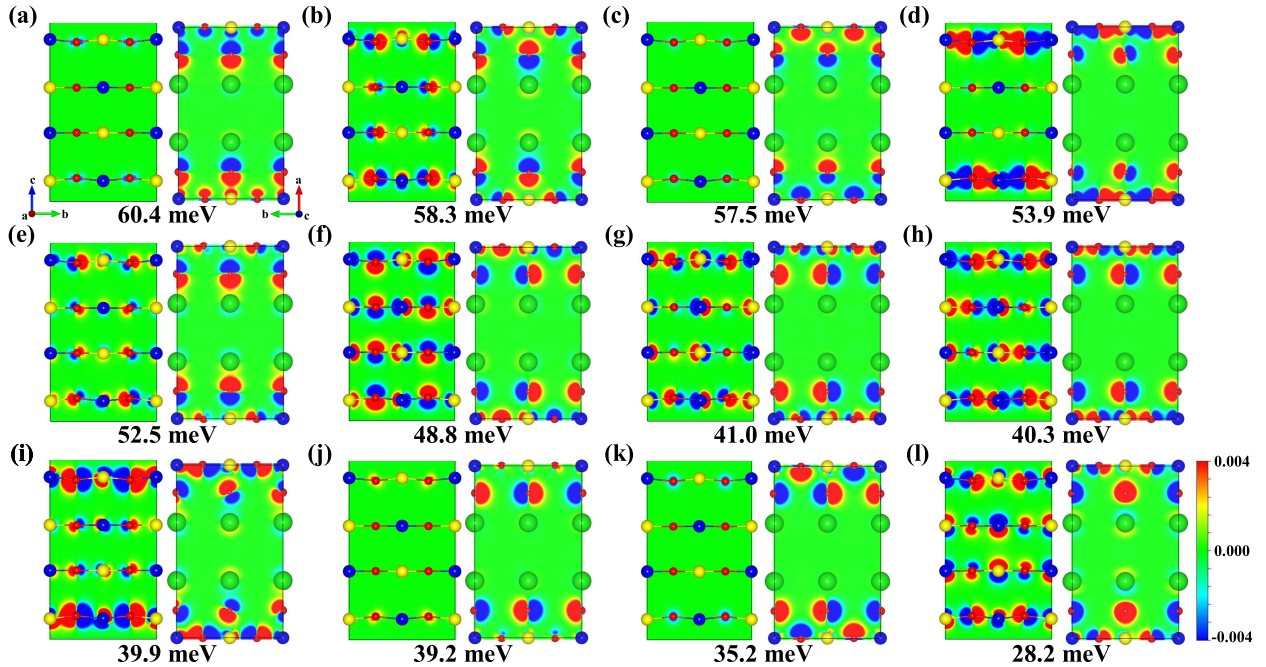


FIG. 6. (Color online) Differential charge density maps of the Sr_2CuO_3 slab in the AFM Néel state between the distorted structures induced by the atomic displacements of different O phonon modes (Fig. 5) and the equilibrium structure plotted on the (100) plane (side view) and the (001) plane (top view). The color bar is in units of $e/\text{Å}^3$.

modes: the mode with in-chain O atoms vibrating along the same direction (Fig. 5d, compared with Fig. 5i) and the modes with neighboring apical O atoms away from or close to the Cu-O chains (Figs. 5a and 5b, compared with Fig. 5e). Besides those modes, other phonon modes with

the out-of-chain O vibrating parallel to the Cu-O chain are also uncovered (Figs. 5f, 5g, 5h, and 5j). Among all above phonon modes considered, the vibrations of out-of-chain O atoms along the a and c axes have the highest and lowest frequencies, respectively.

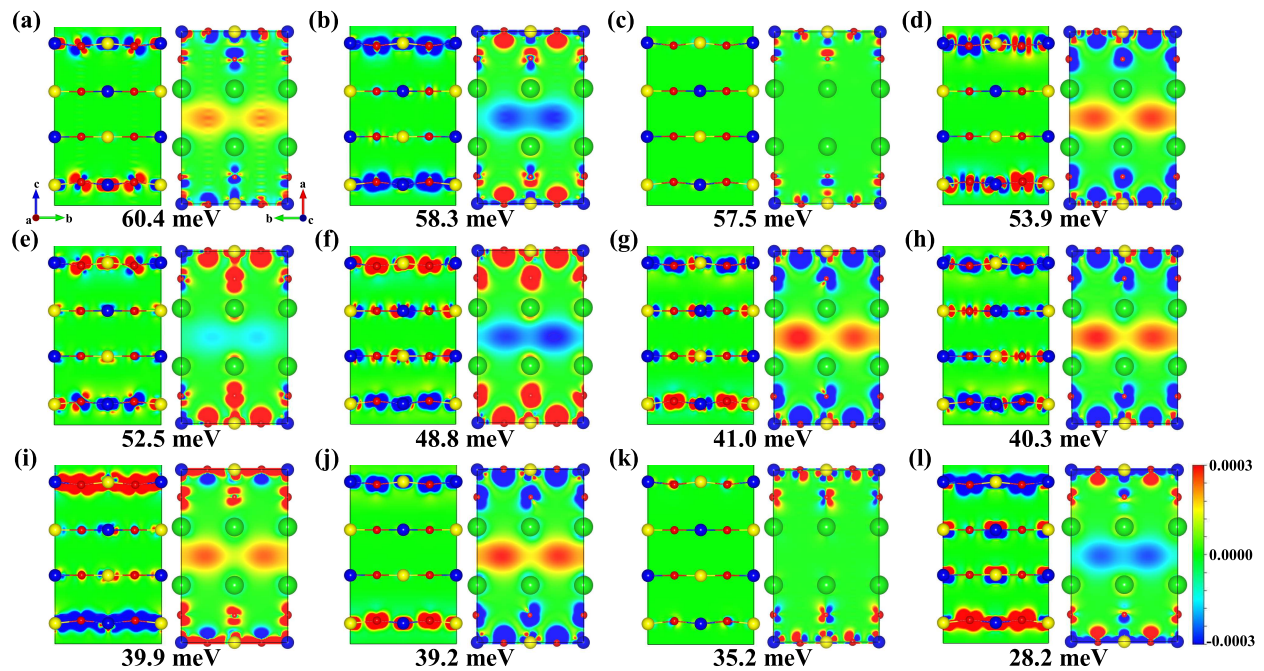


FIG. 7. (Color online) Differential spin density maps of the Sr_2CuO_3 slab in the AFM Néel state between the distorted structure induced by the atomic displacements of different O phonon modes (Fig. 5) and the equilibrium structure plotted on the (100) plane (side view) and the (001) plane (top view). The color bar is in units of $e/\text{\AA}^3$.

In consideration of previous modeling studies on 1D cuprates that have discussed the importance of the bond-stretching and apical O phonons in the *el-ph* interaction [25, 53], here we study the phonon effect on the electronic and magnetic properties for a better understanding of the Cu-O chains on the Sr_2CuO_3 surface. We displaced the atoms in each specific phonon mode s away from the equilibrium position with the corresponding potential energy of $3\hbar\omega_s/2$. To visualize the phonon effect, we plotted the real-space differential charge and spin density maps between the structures with atomic displacements and the one at equilibrium position (Figs. 6, 7, S4, and S5 in the SI [36]). Interestingly, we found that all the phonon modes involving the atomic displacements of O atoms in Fig. 5 can cause significant charge and magnetic fluctuations around the O and Cu atoms on the surface. To be specific, the change of charge density around the O atoms is very obvious; meanwhile the centers of the positive and negative charges do not coincide, indicating the existence of dynamical electrical dipoles on O atoms (Figs. 6 and S4 of SI [36]). To further analyze the charge variations, we calculated the LDOS as a result of the O displacements of above twelve phonon modes (Fig. S6 [36]). As expected, the changes in the density of states of O are largest around the Fermi level, which are consistent with the results in Fig. 6. Notably, we found that the in-chain O vibrations (Figs. 5d and 5i) lead to stronger charge fluctuations (Figs. 6d and 6i) than those of other modes. On the other hand, we notice that there are magnetic fluctuations around Cu and O as well as spin-polarized electron gas between two rows

of surface Sr atoms (Figs. 7 and S5 of SI [36]), where the bond-stretching O phonon mode seems to cause the relatively largest magnetic fluctuations (Figs. 5i and 7i). Here, we attempt to understand why the bond-stretching O phonon (Fig. 5i) causes the most obvious charge and spin fluctuations (Figs. 6i and 7i). There may be two reasons: One is that the vibrations of in-chain O atoms can induce large charge redistributions between Cu and O atoms, thus influencing the charge and spin densities; the other is that according to the displacement formula in the section of COMPUTATIONAL DETAILS, the low frequency of this phonon mode (39.9 meV) corresponds to a large vibrational amplitude, which can directly affect the strength of fluctuations. Based on the above results, besides previous theoretical work that discussed one certain phonon mode contributing to the *el-ph* interaction [25, 53], our results show that more phonon modes involving the vibrations of in-chain and out-of-chain O atoms can induce strong charge and magnetic fluctuations, which may be crucial to understand the properties of 1D cuprates.

C. Modulating the surface properties of Sr_2CuO_3 film by iodine adsorption

In view of the important role of hole doping in cuprate superconductors, we next investigate the adsorption of the iodine (I) atom on the surface of the Sr_2CuO_3 film in order to modulate its electronic properties. As shown in Fig. S7 of SI [36], we considered ten typical adsorption

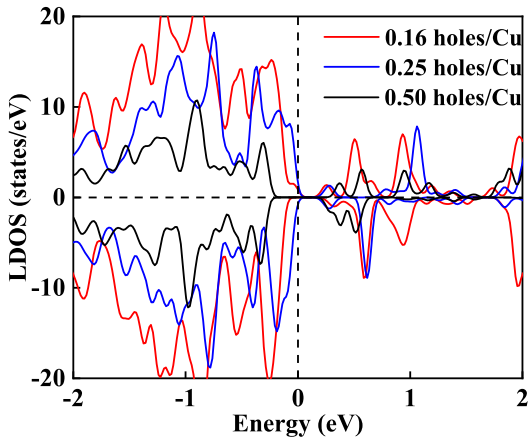


FIG. 8. (Color online) The LDOS for the top surface layer of I-adsorbed Sr_2CuO_3 films at the doping levels of 0.16, 0.25, and 0.50 holes per surface Cu atom.

sites for I atom on the Sr_2CuO_3 surface at the doping level of 0.5 holes per surface Cu atom. According to their relative energies, the most stable structure is that I atom locates directly above Cu14 (Figs. S7f, S8a, and S8d [36]). Then, based on this stable adsorption site of the I atom, the doping levels of 0.25 and 0.167 holes per surface Cu were simulated with the $1 \times 2 \times 1$ and $1 \times 3 \times 1$ supercells, respectively (Fig. S8 [36]).

To study the magnetic and electronic properties of I-adsorbed Sr_2CuO_3 film, we determined the magnetic ground state under different doping levels (Table S5 of SI [36]) and calculated layered-resolved DOSs as in Figs. 8 and S9 of SI [36]. Although the total DOSs all show metallic properties under different doping levels (Figs. S9a-c [36]), we find that the metallicity is mainly derived from the bottom surface layer (7th layer of the slab) (Figs. S9g-i [36]). Unexpectedly, with the increase of hole doping by I atom adsorption, the top surface layer (1st layer of the slab) gradually eliminates its metallicity, exhibiting diverse doped-related magnetic and electronic transitions from antiferromagnetic metal to ferrimagnetic metal and then to ferromagnetic semiconductor (Figs. 8 and S9d-f of SI [36]). Here, we would like to address several points. First, although the DOS seems to be asymmetric at the doping of 0.16 holes/Cu (red line in Fig. 8), actually the Cu atoms are antiferromagnetically coupled and the whole system has a small net magnetic moment (Fig. S9f of SI [36]). Second, the stronger electronegativity of the I atom than that of the Sr atom leads to localized hole doping on the top surface, and therefore this surface cannot maintain the antiferromagnetic ground state at the doping of 0.25 holes per surface Cu (blue line in Fig. 8 and Fig. S9e of SI [36]). Finally, the overdoped cuprates usually show ferromagnetic metal behavior with suppressed superconductivity [54–56]; however, the I-adsorbed Sr_2CuO_3 surface at the doping of 0.5 holes per surface Cu is a ferromagnetic semiconductor (black line in Fig. 8 and Fig. S9d of SI [36]). These

results reflect the effective modulation of spin-polarized electron gas on the surface of Sr_2CuO_3 film by I adsorption.

IV. DISCUSSION AND SUMMARY

The structural, magnetic, electronic, and phonon properties of Sr_2CuO_3 bulk and films have been theoretically investigated. As expected, the bulk Sr_2CuO_3 exhibits the perfect Mott insulator feature (band gap of 1.98 eV) of the cuprate parent compound (Fig. 1c). Subsequently, we focus on the surface of the Sr_2CuO_3 film to study the Cu-O chains directly and have obtained the following results: (1) Unlike the bulk phase, the surface shows metallic properties, and the weak interchain coupling of Cu spins has a large impact on the spin-polarized electron gas between two rows of surface Sr atoms. (2) All phonon modes involving the vibrations of in-chain and out-of-chain O atoms can induce obvious charge and spin fluctuations, which may be crucial to a complete understanding of the superconductivity in 1D cuprates. (3) With the increase of hole doping, the I-adsorbed surface undergoes the transition from antiferromagnetic metal to ferrimagnetic metal and to ferromagnetic semiconductor.

Our computational results and theoretical analyses have identified the spin-polarized electron gas on the surface of the Sr_2CuO_3 film. Note that previous studies have revealed interesting 2D electron gas (2DEG) in the heterostructures. For example, the $\text{LaAlO}_3/\text{SrTiO}_3$ heterostructure has the superconducting 2DEG formed at the interface between two insulating oxides [57]. It is also reported recently that a superconducting stripe state of 2DEG exists at the interface between insulating KTaO_3 and ferromagnetic insulator EuO [58]. Moreover, since the wide-band gap insulator SrTiO_3 is the most common substrate for oxide heterostructures, the 2DEG on the SrTiO_3 surface has also attracted much attention [59]. In fact, the vacuum can be regarded as an insulator, and our work on the Sr_2CuO_3 surface can also be viewed as a study of the interface between two insulators. Surprisingly, we find conductive and controllable spin-polarized electron gas that strongly depends on the coupling between interchain Cu spins. Moreover, we examined the evolution of the spin-polarized surface electron gas with the film thickness. For the 7-layer, 9-layer, and 11-layer Sr_2CuO_3 films, the contours of the spin-polarized surface electron gas look similar when the isosurface values of 3D plots are respectively set to 0.00030, 0.00028, and 0.00026 $\text{e}/\text{\AA}^3$ (Fig. S10 of [36]). This indicates that the spin-polarized surface electron gas decreases slightly with the increasing film thickness, but still remains on the thicker films. We believe that these unusual properties are important for heterostructure phenomena, spintronics application, and even for understanding cuprate superconductivity.

Additionally, we would like to emphasize that the study of Cu-O chains in Sr_2CuO_3 from a phonon per-

spective is indispensable in cuprate superconductors. Although the mechanism of unconventional superconductivity has not reached a consensus, a host of the inelastic neutron scattering (INS) and resonant inelastic x-ray scattering (RIXS) experiments have revealed that magnetic fluctuations in unconventional superconductors are much stronger than those in conventional metals, which suggests that magnetic fluctuations may play an important role in mediating the superconducting pairing [4, 60–63]. On the other hand, numerous ARPES and RIXS experiments as well as theoretical studies have confirmed that some specific phonon modes (e.g., the B_{1g} phonon of $\text{YBa}_2\text{Cu}_3\text{O}_{6+x}$) are associated with unconventional superconducting pairing [64–68]. Here, our calculations on Sr_2CuO_3 not only show that multiple phonon modes can induce strong charge and magnetic fluctuations in Cu-O chains, but also suggest that phonons can effectively couple with other degrees of freedom. Notably, our previous work on infinite-layer SrCuO_2 (with 2D CuO_2 planes) has identified that only the full-breathing phonon mode, involving O in-plane vibrations along the Cu-O bonds, can cause significant fluctuations of local magnetic moments on O atoms and dramatic charge redistributions between Cu and O atoms [47], which is different from present case of Sr_2CuO_3 with 1D Cu-O chains. Although we have not found a uniform law of phonon effect, it is clear that phonon modes in cuprate superconductors with different Cu-O structural units can induce significant charge and spin fluctuations. We draw attention to the important role that phonons play via the couplings with multiple degrees of freedom, which may provide insight to understanding the cuprate superconductivity.

To summarize, we have investigated structural, mag-

netic, electronic, and phonon properties of Sr_2CuO_3 bulk and films based on spin-polarized density functional theory calculations. The bulk phase shows typical Mott insulator features of the cuprate parent compound, while the surface of the Sr_2CuO_3 film shows interesting metallic properties. Through the direct study of Cu-O chains on the Sr_2CuO_3 surface, we find a spin-polarized electron gas between neighboring rows of surface Sr atoms dependent on the coupling of interchain Cu spins. And we find that multiple phonon modes, involving the vibrations of in-chain and out-of-chain O atoms, can induce obvious charge and spin fluctuations. Our work supplies a detailed microscopic picture of the electronic, magnetic, and phonon properties of cuprates containing Cu-O chains, which may facilitate the comprehensive understanding of transition metal oxides with low-dimensional structural units and even of the superconductivity in 1D cuprates.

ACKNOWLEDGMENTS

This work was supported by the National Key R&D Program of China (Grants No. 2022YFA1403103 and No. 2019YFA0308603), the Beijing Natural Science Foundation (Grant No. Z200005), and the National Natural Science Foundation of China (Grants No. 12174443, 11934020, and No. 11004243). K. L. was also supported by the National Key R&D Program of China (Grant No. 2017YFA0302903). Computational resources have been provided by the Physical Laboratory of High Performance Computing at Renmin University of China and the Beijing Super Cloud Computing Center.

-
- [1] M. Nunez-Regueiro, J.-L. Tholence, E. Antipov, J.-J. Capponi, and M. Marezio, Pressure-Induced Enhancement of T_c Above 150 K in Hg-1223, *Science* **262**, 97 (1993).
 - [2] M. Monteverde, C. Acha, M. Núñez-Regueiro, D. Pavlov, K. Lokshin, S. Putilin, and E. Antipov, High-pressure effects in fluorinated $\text{HgBa}_2\text{Ca}_2\text{Cu}_3\text{O}_{8+\delta}$, *EPL* **72**, 458 (2005).
 - [3] A. Yamamoto, N. Takeshita, C. Terakura, and Y. Tokura, High pressure effects revisited for the cuprate superconductor family with highest critical temperature, *Nat. Commun.* **6**, 8990 (2015).
 - [4] B. Keimer, S. A. Kivelson, M. R. Norman, S. Uchida, and J. Zaanen, From quantum matter to high-temperature superconductivity in copper oxides, *Nature* **518**, 179 (2015).
 - [5] A. Damascelli, Z. Hussain, and Z.-X. Shen, Angle-resolved photoemission studies of the cuprate superconductors, *Rev. Mod. Phys.* **75**, 473 (2003).
 - [6] N. Plakida, *High-Temperature Cuprate Superconductors: Experiment, Theory, and Applications* (Springer, Heidelberg, 2010).
 - [7] C.-L. Song, X.-C. Ma, and Q.-K. Xue, Atomic-scale preparation and characterization of high-temperature superconducting thin films (in Chinese), *Sci. China-Phys. Mech. Astron.* **51**, 047402 (2021).
 - [8] D. Li, K. Lee, B. Y. Wang, M. Osada, S. Crossley, H. R. Lee, Y. Cui, Y. Hikita, and H. Y. Hwang, Superconductivity in an infinite-layer nickelate, *Nature* **572**, 624 (2019).
 - [9] J. A. Sobota, Y. He, and Z.-X. Shen, Angle-resolved photoemission studies of quantum materials, *Rev. Mod. Phys.* **93**, 025006 (2021).
 - [10] W. E. Pickett, Electronic structure of the high-temperature oxide superconductors, *Rev. Mod. Phys.* **61**, 433 (1989).
 - [11] A. J. Leggett, What DO we know about high T_c ?, *Nat. Phys.* **2**, 134 (2006).
 - [12] A. P. Petrović, D. Ansermet, D. Chernyshov, M. Hoesch, D. Salloum, P. Gougeon, M. Potel, L. Boeri, and C. Panagopoulos, A disorder-enhanced quasi-one-dimensional superconductor, *Nat. Commun.* **7**, 12262 (2016).
 - [13] K. Y. Arutyunov, D. S. Golubev, and A. D. Zaikin, Superconductivity in one dimension, *Phys. Rep.* **464**, 1 (2008).

- [14] J.-K. Bao, J.-Y. Liu, C.-W. Ma, Z.-H. Meng, Z.-T. Tang, Y.-L. Sun, H.-F. Zhai, H. Jiang, H. Bai, C.-M. Feng, Z.-A. Xu, and G.-H. Cao, Superconductivity in Quasi-One-Dimensional $K_2Cr_3As_3$ with Significant Electron Correlations, *Phys. Rev. X* **5**, 011013 (2015).
- [15] Z. Wang, W. Shi, R. Lortz, and P. Sheng, Superconductivity in 4-Angstrom carbon nanotubes—a short review, *Nanoscale* **4**, 21 (2012).
- [16] R. Y. Chen and N. L. Wang, Progress in Cr- and Mn-based superconductors: a key issues review, *Rep. Prog. Phys.* **82**, 012503 (2019).
- [17] Z. Hiroi, M. Takano, M. Azuma, and Y. Takeda, A new family of copper oxide superconductors $Sr_{n+1}Cu_nO_{2n+1+\delta}$ stabilized at high pressure, *Nature* **364**, 315 (1993).
- [18] S. D. Conradson, T. H. Geballe, C. Jin, L. Cao, G. Baldinozzi, J. M. Jiang, M. J. Latimer, and O. Mueller, Local structure of $Sr_2CuO_{3.3}$, a 95 K cuprate superconductor without CuO_2 planes, *Proc. Natl. Acad. Sci. U.S.A.* **117**, 4565 (2020).
- [19] W.-M. Li, J.-F. Zhao, L.-P. Cao, Z. Hu, Q.-Z. Huang, X.-C. Wang, Y. Liu, G.-Q. Zhao, J. Zhang, Q.-Q. Liu *et al.*, Superconductivity in a unique type of copper oxide, *Proc. Natl. Acad. Sci. U.S.A.* **116**, 12156 (2019).
- [20] Y. Shimakawa and J. Jorgensen, Structural study of $Sr_2CuO_{3+\delta}$ by neutron powder diffraction, *Physica C* **228**, 73 (1994).
- [21] H. Zhang, Y. Wang, L. Marks, V. Dravid, P. Han, and D. Payne, A TEM study of the incommensurate modulated structure in Sr_2CuO_{3+x} superconductors synthesized under high pressure. B. Structural model, *Physica C* **255**, 257 (1995).
- [22] S. D. Conradson, T. H. Geballe, C.-Q. Jin, L.-P. Cao, A. Gauzzi, M. Karppinen, G. Baldinozzi, W.-M. Li, E. Gilioli, J. M. Jiang, M. Latimer, O. Mueller, and V. Nasretdinova, Nonadiabatic coupling of the dynamical structure to the superconductivity in $YSr_2Cu_{2.75}Mo_{0.25}O_{7.54}$ and $Sr_2CuO_{3.3}$, *Proc. Natl. Acad. Sci. U.S.A.* **117**, 33099 (2020).
- [23] K. Liu, Z.-Y. Lu, and T. Xiang, Electronic structures of quasi-one-dimensional cuprate superconductors $Ba_2CuO_{3+\delta}$, *Phys. Rev. Mater.* **3**, 044802 (2019).
- [24] Z. Chen, Y. Wang, S. N. Rebec, T. Jia, M. Hashimoto, D. Lu, B. Moritz, R. G. Moore, T. P. Devereaux, and Zhi-Xun Shen, Anomalously strong near-neighbor attraction in doped 1D cuprate chains, *Science* **373**, 1235 (2021).
- [25] Y. Wang, Z. Chen, T. Shi, B. Moritz, Z.-X. Shen, and T. P. Devereaux, Phonon-mediated long-range attractive interaction in one-dimensional cuprates, *Phys. Rev. Lett.* **127**, 197003 (2021).
- [26] T. Ami, M. Crawford, R. Harlow, Z. Wang, D. Johnston, Q. Huang, and R. Erwin, Magnetic susceptibility and low-temperature structure of the linear chain cuprate Sr_2CuO_3 , *Phys. Rev. B* **51**, 5994 (1995).
- [27] K. Thurber, A. Hunt, T. Imai, and F. Chou, ^{17}O NMR Study of $q = 0$ Spin Excitations in a Nearly Ideal $S = \frac{1}{2}$ 1D Heisenberg Antiferromagnet, Sr_2CuO_3 , up to 800 K, *Phys. Rev. Lett.* **87**, 247202 (2001).
- [28] J. Schlappa, K. Wohlfeld, K. J. Zhou, M. Mourigal, M. W. Haverkort, V. N. Strocov, L. Hozoi, C. Monney, S. Nishimoto, S. Singh *et al.*, Spin-orbital separation in the quasi-one-dimensional Mott insulator Sr_2CuO_3 , *Nature* **485**, 82 (2012).
- [29] J. Schlappa, U. Kumar, K. J. Zhou, S. Singh, M. Mourigal, V. N. Strocov, A. Revcolevschi, L. Patthey, H. M. Rønnow, S. Johnston, and T. Schmitt, Probing multi-spinon excitations outside of the two-spinon continuum in the antiferromagnetic spin chain cuprate Sr_2CuO_3 , *Nat. Commun.* **9**, 5394 (2018).
- [30] P. Hohenberg and W. Kohn, Inhomogeneous electron gas, *Phys. Rev.* **136**, B864 (1964).
- [31] W. Kohn and L. J. Sham, Self-consistent equations including exchange and correlation effects, *Phys. Rev.* **140**, A1133 (1965).
- [32] J. P. Perdew, K. Burke, and M. Ernzerhof, Generalized gradient approximation made simple, *Phys. Rev. Lett.* **77**, 3865 (1996).
- [33] G. Kresse and J. Furthmüller, Efficient iterative schemes for *ab initio* total-energy calculations using a plane-wave basis set, *Phys. Rev. B* **54**, 11169 (1996).
- [34] P. E. Blöchl, Projector augmented-wave method, *Phys. Rev. B* **50**, 17953 (1994).
- [35] H. J. Monkhorst and J. D. Pack, Special points for Brillouin-zone integrations, *Phys. Rev. B* **13**, 5188 (1976).
- [36] See Supplemental Material at <http://link.aps.org/supplemental/10.1103/PhysRevB.110.195121> for the crystal structures and typical spin configurations of bulk Sr_2CuO_3 , optimized crystal structure and LDOS of Sr_2CuO_3 film in the AFM2 state, spin density maps of the Sr_2CuO_3 film plotted on the (001) and (010) planes, differential charge and spin density maps of the film, the surface LDOS of the film as a result of the atomic displacements due to twelve phonon modes in the AFM Néel state, ten typical adsorption sites for I atom on Sr_2CuO_3 surface, the structures and LDOS of the I-adsorbed films at the doping levels of 0.5, 0.25 and 0.167 holes per surface Cu atom, respectively, and the spin density maps of 7-layer, 9-layer, and 11-layer Sr_2CuO_3 slabs.
- [37] H. Suzuura, H. Yasuhara, A. Furusaki, N. Nagaosa, and Y. Tokura, Singularities in optical spectra of quantum spin chains, *Phys. Rev. Lett.* **76**, 2579 (1996).
- [38] N. Motoyama, H. Eisaki, and S. Uchida, Magnetic susceptibility of ideal spin 1/2 Heisenberg antiferromagnetic chain systems, Sr_2CuO_3 and $SrCuO_2$, *Phys. Rev. Lett.* **76**, 3212 (1996).
- [39] K. Maiti, D. D. Sarma, T. Mizokawa, and A. Fujimori, Electronic structure of one-dimensional cuprates, *Phys. Rev. B* **57**, 1572 (1998).
- [40] X. Wu, M. Vargas, S. Nayak, V. Lotrich, and G. Scoles, Towards extending the applicability of density functional theory to weakly bound systems, *J. Chem. Phys.* **115**, 8748 (2001).
- [41] S. Grimme, Semiempirical GGA-type density functional constructed with a long-range dispersion correction, *J. Comput. Chem.* **27**, 1787 (2006).
- [42] F. Ma, Z. Y. Lu, and T. Xiang, Arsenic-bridged antiferromagnetic superexchange interactions in $LaFeAsO$, *Phys. Rev. B* **78**, 224517 (2008).
- [43] F. Ma, W. Ji, J. Hu, Z. Y. Lu, and T. Xiang, First-principles calculations of the electronic structure of tetragonal α -FeTe and α -FeSe crystals: Evidence for a bicolinear antiferromagnetic order, *Phys. Rev. Lett.* **102**, 177003 (2009).
- [44] K. Liu, Z. Y. Lu, and T. Xiang, Nematic antiferromagnetic states in bulk FeSe, *Phys. Rev. B* **93**, 205154 (2016).
- [45] K. Parlinski, Z. Li, and Y. Kawazoe, First-principles de-

- termination of the soft mode in cubic ZrO_2 , *Phys. Rev. Lett.* **78**, 4063 (1997).
- [46] K. Liu and S. Gao, Excitation of frustrated translation and nonadiabatic adatom hopping induced by inelastic tunneling, *Phys. Rev. Lett.* **95**, 226102 (2005).
- [47] X. Du, P.-H. Sun, B.-C. Gong, J.-F. Zhang, Z.-Y. Lu, and K. Liu, Exploring charge and spin fluctuations in infinite-layer cuprate SrCuO_2 from a phonon perspective, *Sci. China Phys. Mech. Astron.* **67**, 287411 (2024).
- [48] T. Olsen, Assessing the performance of the random phase approximation for exchange and superexchange coupling constants in magnetic crystalline solids, *Phys. Rev. B* **96**, 125143 (2017).
- [49] K. Foyevtsova, J. T. Krogel, J. Kim, P. Kent, E. Dagotto, and F. A. Reboredo, *Ab initio* Quantum Monte Carlo calculations of spin superexchange in cuprates: The benchmarking case of Ca_2CuO_3 , *Phys. Rev. X* **4**, 031003 (2014).
- [50] K. Maiti, D. Sarma, T. Mizokawa, and A. Fujimori, Electronic structure of one-dimensional cuprate, Sr_2CuO_3 , *EPL* **37**, 359 (1997).
- [51] T. Manako, Y. Okimoto, M. Izumi, S. Shinomori, M. Kawasaki, H. Kishida, H. Okamoto, T. Fukumura, M. Ohtani, and Y. Tokura, Orientation-controlled epitaxy of A_2CuO_3 (A: Sr, Ca) films with large optical nonlinearity, *Appl. Phys. Lett.* **79**, 1754 (2001).
- [52] B.-J. Zhang, K. Liu, and Z.-Y. Lu, Tuning the magnetism of the top-layer FeAs on $\text{BaFe}_2\text{As}_2(001)$: First-principles study, *Phys. Rev. B* **97**, 165105 (2018).
- [53] S. Li and S. Johnston, Suppressed superexchange interactions in the cuprates by bond-stretching oxygen phonons, *Phys. Rev. B* **108**, L201113 (2023).
- [54] A. Kopp, A. Ghosal, and S. Chakravarty, Competing ferromagnetism in high-temperature copper oxide superconductors, *Proc. Natl. Acad. Sci. U.S.A.* **104**, 6123 (2007).
- [55] K. Kurashima, T. Adachi, K. M. Suzuki, Y. Fukunaga, T. Kawamata, T. Noji, and Y. Koike, Possible ferromagnetic phase in non-superconducting heavily overdoped cuprates of Bi-2201, *J. Phys.: Conf. Ser.* **568**, 022003 (2014).
- [56] T. Sarkar, D. S. Wei, J. Zhang, N. R. Poniatowski, P. R. Mandal, A. Kapitulnik, and R. L. Greene, Ferromagnetic order beyond the superconducting dome in a cuprate superconductor, *Science* **368**, 532 (2020).
- [57] N. Reyren, S. Thiel, A. D. Caviglia, L. Fitting Kourkoutis, G. Hammerl, C. Richter, C. W. Schneider, T. Kopp, A.-S. Rüetschi, D. Jaccard, M. Gabay, D. A. Muller, J.-M. Triscone, and J. Mannhart, Superconducting Interfaces Between Insulating Oxides, *Science* **317**, 1196 (2007).
- [58] X. Hua, Z. Zeng, F. Meng, H. Yao, Z. Huang, X. Long, Z. Li, Y. Wang, Z. Wang, T. Wu, Z. Weng, Y. Wang, Z. Liu, Z. Xiang, and X. Chen, Superconducting stripes induced by ferromagnetic proximity in an oxide heterostructure, *Nat. Phys.* **20**, 957 (2024).
- [59] X. Yan, F. Wrobel, I.-C. Tung, H. Zhou, H. Hong, F. Rodolakis, A. Bhattacharya, J. L. McChesney, and D. D. Fong, Origin of the 2D Electron Gas at the SrTiO_3 Surface, *Adv. Mater.* **34**, 2200866 (2022).
- [60] M. Le Tacon, G. Ghiringhelli, J. Chaloupka, M. Moretti Sala, V. Hinkov, M. W. Haverkort, M. Minola, M. Bakr, K. J. Zhou, S. Blanco-Canosa *et al.*, Intense paramagnon excitations in a large family of high-temperature superconductors, *Nat. Phys.* **7**, 725 (2011).
- [61] M. P. M. Dean, G. Dellea, R. S. Springell, F. Yakhov-Harris, K. Kummer, N. B. Brookes, X. Liu, Y.-J. Sun, J. Strle, T. Schmitt *et al.*, Persistence of magnetic excitations in $\text{La}_{2-x}\text{Sr}_x\text{CuO}_4$ from the undoped insulator to the heavily overdoped non-superconducting metal, *Nat. Mater.* **12**, 1019 (2013).
- [62] H. F. Fong, P. Bourges, Y. Sidis, L. P. Regnault, J. Bossy, A. Ivanov, D. L. Milius, I. A. Aksay, and B. Keimer, Spin susceptibility in underdoped $\text{YBa}_2\text{Cu}_3\text{O}_{6+x}$, *Phys. Rev. B* **61**, 14773 (2000).
- [63] P. Dai, H. A. Mook, R. D. Hunt, and F. Doğan, Evolution of the resonance and incommensurate spin fluctuations in superconducting $\text{YBa}_2\text{Cu}_3\text{O}_{6+x}$, *Phys. Rev. B* **63**, 054525 (2001).
- [64] Z.-X. Shen, A. Lanzara, S. Ishihara, and N. Nagaosa, Role of the electron-phonon interaction in the strongly correlated cuprate superconductors, *Philos. Mag.* **B 82**, 1349 (2002).
- [65] X. J. Zhou, T. Cuk, T. Devereaux, N. Nagaosa, and Z.-X. Shen, in *Handbook of High-Temperature Superconductivity: Theory and Experiment*, edited by J. R. Schrieffer and J. S. Brooks (Springer, New York, 2007), Chap. 3, p. 87.
- [66] T. P. Devereaux, T. Cuk, Z. X. Shen, and N. Nagaosa, Anisotropic electron-phonon interaction in the cuprates, *Phys. Rev. Lett.* **93**, 117004 (2004).
- [67] C. Jiang, E. Beneduce, M. Baggioli, C. Setty, and A. Zaccane, Possible enhancement of the superconducting due to sharp Kohn-like soft phonon anomalies, *J. Phys.: Condens. Matter* **35**, 164003 (2023).
- [68] J. Li, A. Nag, J. Pellicciari, H. Robarts, A. Walters, M. Garcia-Fernandez, H. Eisaki, D. Song, H. Ding, S. Johnston, R. Comin, and K.-J. Zhou, Multiorbital charge-density wave excitations and concomitant phonon anomalies in $\text{Bi}_2\text{Sr}_2\text{LaCuO}_{6+\delta}$, *Proc. Natl. Acad. Sci. U.S.A.* **117**, 16219 (2020).